ENVIRONMENTAL RESEARCH
LETTERS

CrossMark

OPEN ACCESS

RECEIVED
20 October 2023

REVISED
5 March 2024

ACCEPTED FOR PUBLICATION
7 March 2024

PUBLISHED
15 March 2024

PERSPECTIVE

Heat index extremes increasing several times faster than the air temperature

David M Romps

Department of Earth and Planetary Science, University of California, Berkeley, CA, United States of America
Climate and Ecosystem Sciences Division, Lawrence Berkeley National Laboratory, Berkeley, CA, United States of America

E-mail: romps@berkeley.edu

Keywords: global warming, heat index, heat stress

Supplementary material for this article is available online

Many effects of global warming are far removed from the average person's experience, but anthropogenic global warming is exacerbating heat stress for billions of people where they live today (Mastrucci *et al* 2019, Raymond *et al* 2020, Baldwin *et al* 2023), reducing labor capacity (Dunne *et al* 2013), and increasing heat-induced mortality (Vicedo-Cabrera *et al* 2021). Therefore, public communication of global warming's heat-stress implications can serve two important purposes: promoting life-saving adaptation and raising awareness of the benefits of warming mitigation (Patz *et al* 2014, Koh 2016, Cvijanovic *et al* 2023).

To communicate the contribution of global warming to an observed heat event, one approach is to calculate how much more likely the event was to exceed a fixed temperature threshold (Shepherd 2016). While this approach can lead to statements that the probability of exceeding a fixed temperature has, e.g. doubled (Stott *et al* 2004), it is often more appropriate to report the change in temperature at a fixed probability of exceedance (e.g. Perkins-Kirkpatrick *et al* 2022). Those changes in temperature are typically more modest-sounding because, for more than 90% of the land area between 60 °S and 60 °N, global warming has increased average daily-maximum temperatures by less than 2 °C (calculated using Berkeley Earth; see supplementary material 1.1). On the other hand, we will argue that these relatively modest-sounding changes in temperature have caused large increases in heat stress as quantified by the heat index. Focusing on Texas as a case study, we will show that global warming increased the highest heat index during June, July, and August (JJA) of 2023 by, on average, ∼5–6 °C (∼8–11 °F).

Because of the evaporative cooling of sweat, heat stress is influenced not just by the air temperature, but also by humidity. All else equal, higher humidity reduces evaporative cooling and, therefore, increases heat stress, as clearly evidenced by laboratory studies (e.g. Wolf *et al* 2022). While there are many different metrics of heat stress in use (Havenith and Fiala 2015), the heat index stands out for its basis in physiological modeling (Steadman 1979) and its validation against laboratory experiments (Lu and Romps 2023).

Given the actual air temperature T and water–vapor pressure p_v, the heat index is the air temperature that would feel the same at a reference vapor pressure of 1.6 kPa (Steadman 1979, Lu and Romps 2022). Although the heat index is often called a 'feels like' temperature, the heat index is based on a model of physiology, not psychology: the heat index is the temperature at 1.6 kPa that would generate the same physiological response as the actual T and p_v. In other words, the heat index $T_{\rm HI}$ is defined implicitly by

$$\text{physiology}\left(T_{\rm HI}, 1.6\,\text{kPa}\right) = \text{physiology}\left(T, p_v\right)\,. \quad (1)$$

Under the hood, the heat index runs on a mathematical model of human thermoregulation. Originally calculated up to the point where sweat begins to drip off the skin (Steadman 1979), the calculation has since been extended to all combinations of temperature and humidity (Lu and Romps 2022). While there have been many studies of global warming's impact on the heat index, studies have relied on a polynomial extrapolation of originally calculated values (Rothfusz 1990). That extrapolation has errors as large as 10 °C (Romps and Lu 2022) and so is not used here. Instead, we calculate the heat index by solving the equations of its underlying thermoregulatory model (Lu and Romps 2022).

To estimate the impact of global warming on the heat index, we need to know how its two inputs—temperature and humidity—are changing. Any realistic change to the climate will alter mean diurnal

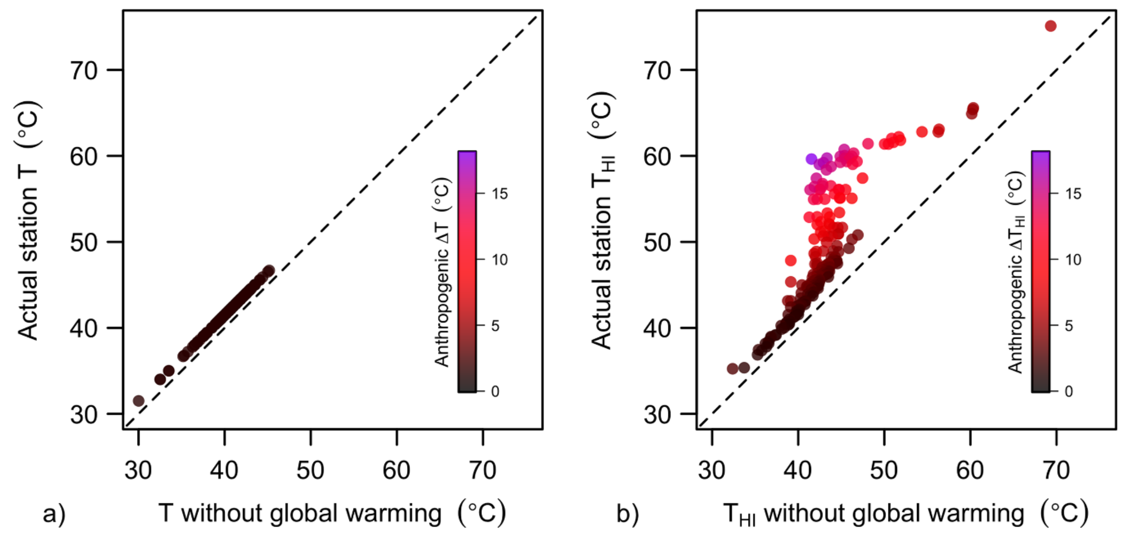

Figure 1. (a) Maximum temperature at each ASOS station in Texas during JJA 2023, plotted against the approximate temperature it would have been in the absence of global warming, which is 1.5 °C lower than observed. (b) Maximum heat index at each ASOS station in Texas during JJA 2023, plotted against the approximate heat index it would have been in the absence of global warming (calculated by subtracting 1.5 °C from the temperature while holding relative humidity fixed). For visual reference, the one-to-one line is marked by a dashed curve in both panels. Colors denote the approximate global-warming impact: the difference between the observed value and the approximate value it would have been in the absence of global warming.

cycles as well as distributions of daily-minimum and daily-maximum temperatures. To first approximation, however, we can model the changes to a temperature distribution as if it were simply shifted by the change in its mean (Simolo *et al* 2011, McKinnon *et al* 2016). In this spirit, a weather station's temperature reading can be mapped to the value it would have been in the absence of global warming by subtracting from it the mean change in temperature from preindustrial to the present. Here, we approximate the local effect of global warming by the observed change in decadal-mean local temperature. Likewise, to first approximation, the distribution of relative humidity does not change with global warming (Held and Soden 2006, Schneider *et al* 2010). Therefore, given an observation of T and RH, we can approximate the conditions that would have prevailed in the absence of global warming, all else equal, by subtracting the mean warming from T and leaving RH unchanged.

To illustrate the effect of this mapping on the heat index, we will focus on Texas as a case study. The area-weighted average of daily-mean Texas surface-air temperatures during JJA has warmed by 1.5 °C from preindustrial (1850–1859) to present (2013–2022) (Berkeley Earth; see SM 1.1). To analyze the recent heat extremes in Texas, we use hourly Automated Surface Observing Systems (ASOS) station data archived by the Iowa Environmental Mesonet (see SM 1.2). There were 210 stations reporting temperature and relative humidity from June 1 to August 31 of 2023 (see table S1). For each station, we calculate its maximum hourly mean temperature and maximum hourly mean heat index (Lu and Romps 2022) during those three months. To calculate changes in these quantities since the preindustrial, we are unable to use ASOS time series directly because the median age of ASOS stations is only 20 yr. Instead, for each station, we can estimate what the maximum heat index in JJA 2023 would have been in the absence of global warming, i.e. if the relative humidities had been the same, but if all the temperatures had been lower by 1.5 °C.

Figure 1(a) plots each station's maximum temperature during JJA 2023 against that same temperature minus 1.5 °C. Here, the approximate impact of global warming on maximum temperatures is visualized by the departure of the points from the one-to-one line, shown by the dashed curve. Figure 1(b) plots each station's maximum heat index (during JJA 2023) against the maximum heat index that would have been achieved if temperatures were 1.5 °C cooler, i.e. in the absence of global warming. This plot allows us to see how global warming has affected recent heat-index values. At lower temperatures, the effect of humidity on physiology becomes less pronounced, and T_{HI} asymptotes to T. Consistent with this, at lower values on the abscissa, the points are elevated above the one-to-one line by close to 1.5 °C, similar to figure 1(a). At higher values on the abscissa, however, we see large departures from the one-to-one line. For example, the highest observed heat index of 75 °C (at Houston's Ellington Airport on July 23) would have been about 6 °C lower at a value of 69 °C in the absence of global warming. Assuming constant relative humidity, the 1.5 °C of global warming has increased these maximum heat-index values by an average of 6 °C.

A heat index of 75 °C might sound unrealistic and unsurvivable, but it is, in fact, both realistic and—for a young, healthy individual—survivable. To understand why, we must recall that the heat index is the physiologically equivalent temperature, assuming wetted skin, at a reference water–vapor pressure of 1.6 kPa. For comparison, at 1.6 kPa, an air temperature of 75 °C has a wet-bulb temperature of only 31 °C (see SM 1.3 and figure S1). The energy budget of a wet human is similar to that of a wet bulb: in both cases, the temperature of the wetted surface is largely set by the need to balance sensible and radiant heat flowing in and latent heat flowing out. For a person, however, there is the additional metabolic heat that must be shed to the environment, leading to a somewhat higher temperature of the wetted surface for a sweaty person than for a wet bulb. In particular, 75 °C and 1.6 kPa induces (for a young, healthy person in steady-state heat balance) a skin temperature of 38 °C, which is far less than 75 °C, and which corresponds to a dangerous, but survivable, state of hyperthermia. Thus, the large latent heat of water postpones hyperthermia to a high value of the heat index for the same reason that the wet-bulb temperature can deviate by several tens of degrees from the dry-bulb temperature.

Although the very high heat index of 75 °C was bumped up by global warming by ∼6 °C, some other heat-index values were affected much more. For example, on June 20, 2023, the city of Nacogdoches had an hourly mean heat index of 60 °C. At the time, the temperature was 31 °C with a relative humidity of 91%. Had the relative humidity been the same, but the temperature lower by 1.5 °C, the heat index would have been lower by 18 °C. This large sensitivity to temperature is caused by the heat and humidity approaching those conditions that would induce hyperthermia in a young, healthy adult. According to the heat index model, in the conditions at Nacogdoches, the global-warming-induced temperature increase of 1.5 °C increased a person's skin blood flow by 0.5 l min^{-1} (compared to a basal rate of about 0.6 l min^{-1}) so as to avoid hyperthermia. At 1.6 kPa, the temperature would need to increase by 18 °C (from 42 °C to 60 °C) to induce the same physiological stress (i.e. the same skin blood flow; see SM 1.4 and figure S2). This high sensitivity is caused by the approach to the physiological limit: for the observed relative humidity of 91%, no amount of skin blood flow can prevent hyperthermia at temperatures over 34 °C (Lu and Romps 2022).

To corroborate these estimated changes in the heat index, we can turn next to the ERA5 reanalysis (Hersbach *et al* 2020). We use hourly data in the local afternoon (17 UTC to 22 UTC) during all days of JJA from grid cells centered within Texas from 1942 to 2023 (values for 1940 and 1941 were discarded as outliers; see SM 1.5 and figure S3). In the analysis of the ASOS station data, we used two approximations that we can check using the ERA5 data: 1. that the temperatures at the time of maximal heat index have been affected by global warming the same as the mean annual temperature, and 2. that the relative humidities at the time of maximal heat index have remained roughly constant. In the ERA5 data, the temperature at the time of each grid cell's annual maximum heat index increased, from 1942–1951 to 2014–2023, by an average of 0.8 K, which is nearly identical to the mean annual temperature increase during that time (1.0 K from ERA5 and 0.9 K from Berkeley Earth), corroborating the first approximation. Regarding the second approximation, the average relative humidity at the time of the maximal heat index did not decrease: in fact, it actually increased slightly, from 31% to 35%.

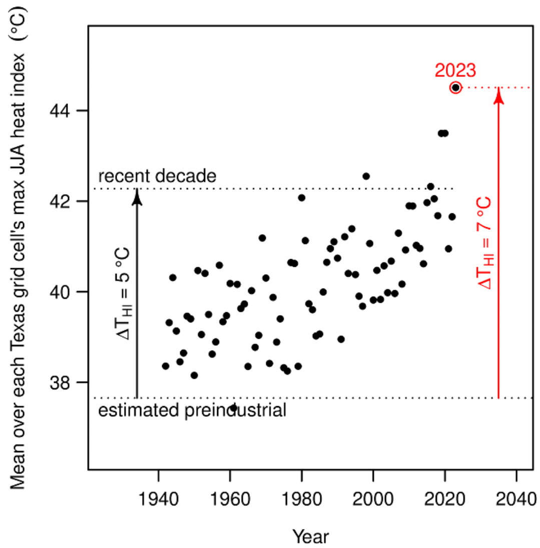

Figure 2. For each year of ERA5 data from 1942 to 2023, the mean over each Texas grid point's maximum hourly heat index from the hours of 17–22 UTC during JJA. The top dashed line marks the mean of the data points 2014–2023. The lower dashed line marks the estimate of the preindustrial mean (of maximum heat index) obtained using ERA5 and Berkeley Earth.

In the analysis of ERA5 heat index, we do not need to use either of those two approximations because we can calculate the time series of the heat index directly. Overall, the mean of the annual grid-point maximum heat index increased in ERA5 from 1942–1951 to 2013–2022 by 3 °C. To estimate the change since preindustrial, we can multiply this number by the warming since preindustrial divided by the warming since 1942–1951, which gives a mean increase in maximum heat index of 5 °C. This is illustrated in figure 2, which plots the mean (over grid cells) of annual maximum heat index. In 2023, this mean was 7 °C above preindustrial. In summary, both station data and reanalysis are consistent with global warming having increased the most extreme values of the heat index in Texas by ∼5–6 °C (∼8–11 °F).

In public communications, global warming is typically quantified in terms of the dry-bulb temperature, but that fails to convey the true impact on heat stress. A person's typical experience of diurnal temperature variations is in association with approximately constant specific humidity, biasing the perception of the implications of +1.5 °C. Global warming, on the other hand, can generate temperature increases with roughly constant, or even increasing, relative humidity. At an air temperature of 30 °C and 90% relative humidity, a 1.5 °C increase in air temperature at fixed *specific* humidity increases a person's skin blood flow by about 12%. On the other hand, with a more realistic depiction of global warming as occurring with fixed *relative* humidity, that same 1.5 °C increase in air temperature increases a person's skin blood flow by 58%. The heat index rises by 15 °C in this case, reflecting the approach to hyperthermic conditions and the amplification of heat stress from constant relative humidity. Communicating the impact of global warming in terms of changes to the heat index gives the public a more accurate picture of the extent to which global warming has increased heat stress.

Data availability statement

No new data were created or analysed in this study.

Conflict of interest

The author declares no competing interests.

ORCID iD

David M Romps https://orcid.org/0000-0001-7649-5175

References

Baldwin J W, Benmarhnia T, Ebi K L, Jay O, Lutsko N J and Vanos J K 2023 Humidity's role in heat-related health outcomes: a heated debate *Environ. Health Perspect.* **131** 055001

Cvijanovic I, Mistry M N, Begg J D, Gasparrini A and Rodó X 2023 Importance of humidity for characterization and communication of dangerous heatwave conditions *npj Clim. Atmos. Sci.* **6** 33

Dunne J P, Stouffer R J and John J G 2013 Reductions in labour capacity from heat stress under climate warming *Nat. Clim. Change* **3** 563–6

Havenith G and Fiala D 2015 Thermal indices and thermophysiological modeling for heat stress *Compr. Physiol.* **6** 255–302

Held I M and Soden B J 2006 Robust responses of the hydrological cycle to global warming *J. Clim.* **19** 5686–99

Hersbach H *et al* 2020 The ERA5 global reanalysis *Q. J. R. Meteorol. Soc.* **146** 1999–2049

Koh H 2016 Communicating the health effects of climate change *JAMA* **315** 239–40

Lu Y-C and Romps D M 2022 Extending the heat index *J. Appl. Meteorol. Clim.* **61** 1367–83

Lu Y-C and Romps D M 2023 Predicting fatal heat and humidity using the heat index model *J. Appl. Physiol.* **134** 649–56

Mastrucci A, Byers E, Pachauri S and Rao N D 2019 Improving the SDG energy poverty targets: residential cooling needs in the global South *Energy Build.* **186** 405–15

McKinnon K A, Rhines A, Tingley M P and Huybers P 2016 The changing shape of Northern Hemisphere summer temperature distributions *J. Geophys. Res.: Atmos.* **121** 8849–68

Patz J A, Frumkin H, Holloway T, Vimont D J and Haines A 2014 Climate change: challenges and opportunities for global health *JAMA* **312** 1565–80

Perkins-Kirkpatrick S E, Stone D A, Mitchell D M, Rosier S, King A D, Lo Y T E, Pastor-Paz J, Frame D and Wehner M 2022 On the attribution of the impacts of extreme weather events to anthropogenic climate change *Environ. Res. Lett.* **17** 024 009

Raymond C, Matthews T and Horton R M 2020 The emergence of heat and humidity too severe for human tolerance *Sci. Adv.* **6** eaaw1838

Romps D M and Lu Y-C 2022 Chronically underestimated: a reassessment of US heat waves using the extended heat index *Environ. Res. Lett.* **17** 094 017

Rothfusz L P 1990 The heat index "equation" (or, more than you ever wanted to know about heat index) *Technical Attachment SR 90-23* NWS Southern Region Headquarters, Forth Worth, TX

Schneider T, O'Gorman P A and Levine X J 2010 Water vapor and the dynamics of climate changes *Rev. Geophys.* **48** RG3001

Shepherd T G 2016 A common framework for approaches to extreme event attribution *Curr. Clim. Change Rep.* **2** 28–38

Simolo C, Brunetti M, Maugeri M and Nanni T 2011 Evolution of extreme temperatures in a warming climate *Geophys. Res. Lett.* **38** L16701

Steadman R G 1979 The assessment of sultriness. Part I: a temperature-humidity index based on human physiology and clothing science *J. Appl. Meteorol.* **18** 861–73

Stott P A, Stone D A and Allen M R 2004 Human contribution to the European heatwave of 2003 *Nature* **432** 610–4

Vicedo-Cabrera A M *et al* 2021 The burden of heat-related mortality attributable to recent human-induced climate change *Nat. Clim. Change* **11** 492–500

Wolf S T, Cottle R M, Vecellio D J and Kenney W L 2022 Critical environmental limits for young, healthy adults (PSU HEAT Project) *J. Appl. Physiol.* **132** 327–33

Supplementary Material for "Heat index extremes increasing several times faster than the air temperature"

David M. Romps[1 2 *]

1 Methods

1.1 Warming

Data from Berkeley Earth were used to reach the conclusion that, for more than 90% of the land area between 60° S and 60° N, global warming has increased average daily-maximum temperatures by less than 2 °C. The data used are referred to as Global Monthly Land High Temperature (TMAX; 1833-Recent) $1° \times 1°$ Latitude-Longitude Grid (filename `Complete_TMAX_LatLong1.nc` available at `https://berkeleyearth.org/data`). To represent the preindustrial, the decade of 1900-1909, inclusive, was chosen; data availability was deemed too sparse globally in previous decades of this dataset. To represent the modern, the decade of 2012-2021, inclusive, was used. Restricting to grid points over land with a latitude between 60° S and 60° N, the surface-air temperature was averaged over these two decades for each grid point and the difference taken. Weighted quantiles of these differences were calculated (using the grid-cell area as the weight) and the value at the 90th percentile was recorded, which was 1.9 °C. Data from Berkeley Earth were also used to reach the conclusion that the area-weighted average of daily-mean Texas surface-air temperatures during JJA has warmed by 1.5 °C from preindustrial (1850-1859) to present (2013-2022). The data used are referred to as $1° \times 1°$ Gridded Monthly Average Temperature (1850-Recent) Contiguous USA (filename `CONUS_TAVG_Gridded_1.nc` available at `https://berkeleyearth.org/data`). Restricting to JJA and grid points centered inside Texas, the grid-cell-area weighted mean of temperature was averaged over 1850-1859, inclusive, and 2013-2022, inclusive. The difference of the means equals 1.5 °C.

1.2 Station data

Hourly data from Texas Automated Surface Observing Systems (ASOS) stations were obtained from the Iowa Environmental Mesonet at `https://mesonet.agron.iastate.edu/request/download.phtml?network=TX_ASOS`. There were 210 stations with coincident valid values of temperature and relative humidity during JJA 2023. The stations are listed in Table S1. For each of these stations, the maximum hourly temperature during JJA 2023 was identified. Independently, the heat index was calculated for every hour at each station and, for each station, the highest hourly heat index during JJA 2023 was identified. Finally, the hourly heat index values were recalculated using the same relative humidities with temperatures lowered by 1.5 °C, and the maximum of those values for each station was identified. For the calculation of the heat index, solutions of the thermoregulatory model were used (Lu and Romps, 2022) rather than an inaccurate polynomial extrapolation (Rothfusz, 1990).

1.3 Wet-bulb temperature

Some surprisingly high air temperatures can be survivable so long as the relative humidity is sufficiently low, the air is moving at a moderate speed or better, and the skin is kept wetted. The reason for this survivability is that the evaporative cooling of a wetted body increases rapidly with the air temperature at constant specific humidity or vapor pressure. This phenomenon is present in the physiological model underlying the heat index, but is also present in the simpler physics of a psychrometric wet bulb (for which there is no metabolic heat and the wind speed is large enough that radiative fluxes can be neglected). Figure S1 plots the wet-bulb temperature at constant vapor pressure ($p_v = 1.6$ kPa, typical of spaces conditioned

[1]Department of Earth and Planetary Science, University of California, Berkeley, California
[2]Climate and Ecosystem Sciences Division, Lawrence Berkeley National Laboratory, Berkeley, California
[*]email: romps@berkeley.edu

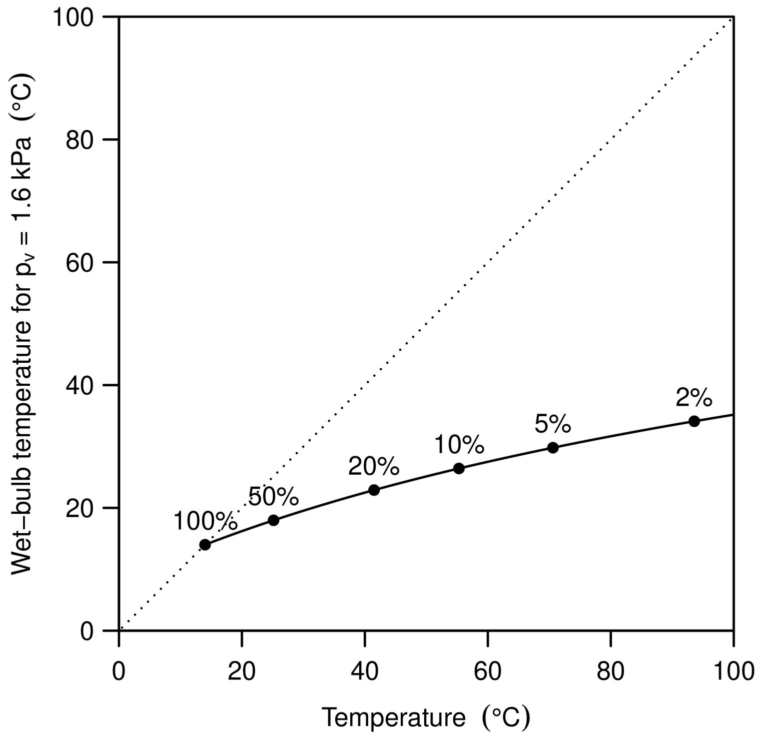

Figure S1: For a water-vapor pressure of 1.6 kPa, (solid curve) the wet-bulb temperature as a function of dry-bulb temperature. The circles and associated percentages give the relative humidity at the corresponding pairs of dry-bulb and wet-bulb temperatures. The dotted curve is the 1-to-1 line, shown for visual reference.

for humans) as a function of the air temperature. Note that the temperature of the wet bulb increases much more slowly than the air temperature. For example, at an air temperature of 75 °C, the temperature of the wet bulb is only 31 °C.

1.4 Skin blood flow

In the heat index model of thermoregulation, the variable R_s is the resistance to heat transfer through the skin (Steadman, 1979). In regions IV and V of heat stress (IV = naked, V = dripping sweat), R_s is the variable that the body modulates to maintain a normal core temperature. The body achieves this by altering the rate of skin blood flow, flushing the skin with blood when under heat stress so as to raise the skin temperature to more effectively shed heat. Here, the heat index model (Lu and Romps, 2022) is used along with an equation (Gagge et al., 1972) that relates R_s to the skin blood flow.

Warming can increase the heat index by many multiples of the increase in air temperature. For example, the inferred increase in temperature of 1.5 °C in Nacogdoches, Texas on June 20, 2023 led to an 18 °C increase in the heat index. Recalling that the heat index is the air temperature at $p_v = 1.6$ kPa that would produce the same heat stress as the prevailing conditions, the reason for the 18 °C jump in the heat index is illustrated in Figure S2.

1.5 Reanalysis

ERA5 data were obtained from the Copernicus Climate Change Service, requesting hourly surface pressure, 2-m temperature, and 2-m dewpoint temperature over a small domain encompassing Texas from five hours in the local afternoon (17-22 UTC) for all days in June, July, and August from June 1, 1940 to August 31, 2023, available at `cds.climate.copernicus.eu`. The annual ERA5 Texas JJA-afternoon-mean temperatures for

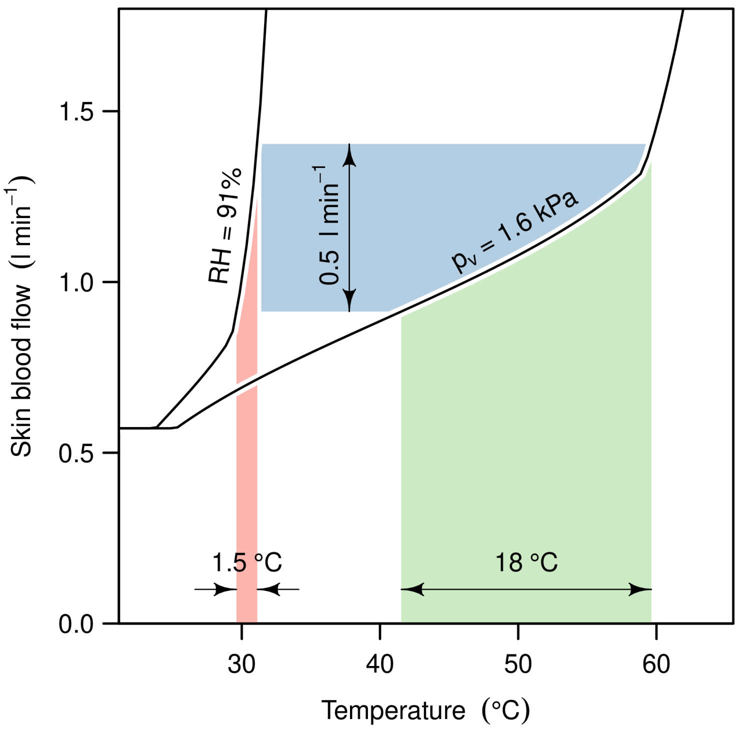

Figure S2: According to the thermoregulation model underpinning the heat index, the skin blood flow required to maintain a normal core temperature at two levels of humidity: RH = 91% (the value at the time of the heat index of 60 °C recorded in Nacogdoches, Texas on June 20, 2023) and $p_v = 1.6$ kPa (the reference vapor pressure used to define the heat index). At the time of the 60 °C heat index, the air temperature was 31 °C. Global warming has raised the counterfactual temperature of 29.5 °C by about 1.5 °C to that value of 31 °C (red shading), which has caused the required skin blood flow at 91% relative humidity to increase by 0.5 liters per minute (blue shading), which is equivalent to raising the temperature by 18 °C at the reference vapor pressure of 1.6 kPa (green shading).

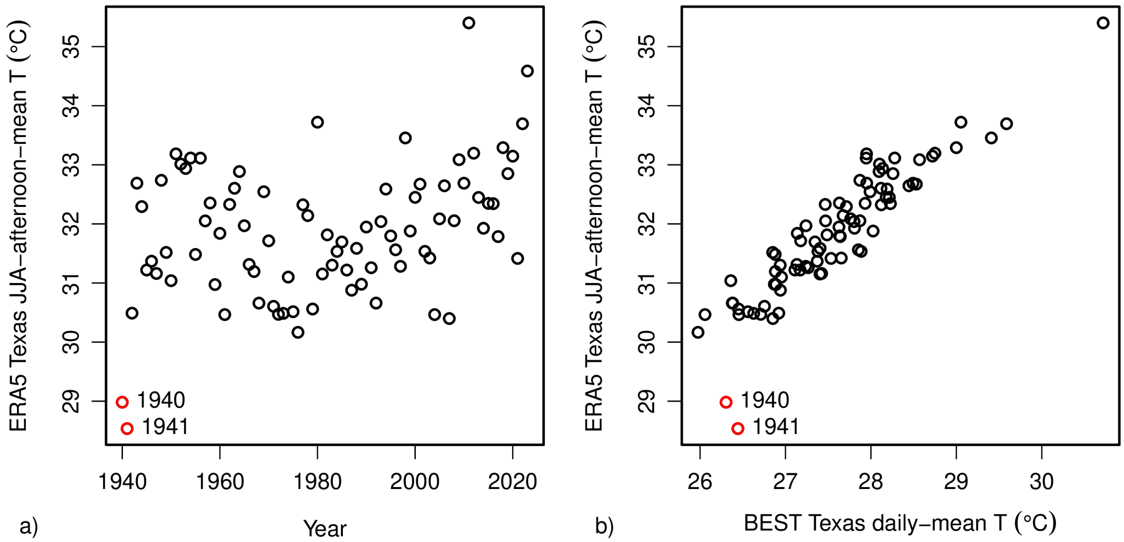

Figure S3: (a) The time series of annual ERA5 Texas JJA-afternoon-mean temperature. (b) The annual ERA5 Texas JJA-afternoon-mean temperature plotted against the annual BEST Texas daily-mean temperature. In both panels, the ERA5 values for 1940 and 1941, highlighted in red, are outliers.

the first two years of the ERA5 record (1940 and 1941) are evident as outliers both when the ERA5 mean values are plotted as time series (Figure S3a) and when the same data are plotted against annual BEST Texas daily-mean temperature (Figure S3b). Therefore, those two years are removed from the ERA5 data analysis.

The relative humidity was calculated as the ratio of the saturation vapor pressure for the 2-m dewpoint temperature to the saturation vapor pressure for the 2-m temperature. The heat index was calculated from the 2-m temperature and relative humidity (Lu and Romps, 2022). Code for calculating the heat index and skin blood flow is available at `https://romps.berkeley.edu/papers/pubs-2020-heatindex.html`. To calculate the mean of the maximum Texas grid-point JJA afternoon heat index values for a given year, the maximum value of the heat index was calculated for each Texas grid point (during the 5 hours in JJA) for each year from 1942 to 2023, and the mean of those maximum grid-point values was calculated for each year.

Table S1: Meteorological stations in Texas

ID	Station	Longitude	Latitude
EFD	HOUSTON/ELLINGTON	−95.15875	29.60733
HQZ	MESQUITE	−96.53042	32.74696
SKF	KELLY AFB	−98.58111	29.38423
BAZ	NEW BRAUNFELS MUNI APT (WAS 3R5)	−98.04500	29.70900
T69	Sinton	−97.54250	28.03860
BYY	BAY_CITY	−95.86344	28.97325
NQI	KINGSVILLE NAS	−97.80970	27.50720
NFW	FORT WORTH NAS	−97.43648	32.78098
JAS	JASPER COUNTY−BELL FIELD AIRPORT	−94.03494	30.88569
CRP	CORPUS CHRISTI INTL	−97.51278	27.77306
8T6	George West / Live Oak	−98.11650	28.36280
ELA	Eagle Lake	−96.32190	29.60060
6R3	Cleveland	−95.00800	30.35644

continued on next page

Table S1: Continued from previous page

ID	Station	Longitude	Latitude
BKS	FALFURRIAS/BROOKS COUNTY AIRPORT	−98.12111	27.20667
ARM	WHARTON REGIONAL ARPT	−96.15439	29.25428
RBO	ROBSTOWN	−97.69052	27.77854
INJ	HILLSBORO	−97.09722	32.08361
ALI	ALICE INTL AIRPORT	−98.02694	27.74089
3T5	LA GRANGE/FAYETTE REGIONAL	−96.95000	29.91000
5T9	Maverick County	−100.51350	28.85710
DKR	Crocket	−95.40383	31.30696
EBG	EDINBURG	−98.12222	26.44167
OCH	NACOGDOCHES (AWOS)	−94.70944	31.57778
IKG	Kingsville	−98.03090	27.55090
PWG	MC GREGOR (AWOS)	−97.31653	31.48492
CPT	CLEBURNE	−97.43375	32.35375
NGP	CORPUS CHRISTI NAS	−97.29109	27.69263
MFE	MCALLEN/MILLER INTL	−98.23861	26.17583
PRX	PARIS/COX FIELD	−95.45075	33.63661
PSX	PALACIOS MUNICIPAL	−96.25000	28.73000
T78	Liberty	−94.69860	30.07780
MKN	COMANCHE COUNTY/CITY ARPT	−98.60000	31.92000
OSA	MOUNT PLEASANT AIRPORT	−94.96139	33.09556
LFK	LUFKIN/ANGELINA CO.	−94.75000	31.23401
VCT	VICTORIA REGIONAL	−96.93030	28.86140
HRL	HARLINGEN INTL ARPT	−97.65439	26.22850
F00	Bonham	−96.17930	33.61310
UVA	UVALDE/GARNER_FIELD_ARPT	−99.74358	29.21133
NOG	ORANGE GROVE	−98.05167	27.90113
HDO	HONDO MUNICIPAL	−99.17417	29.35944
BPT	Beaumont − Port Arthur	−94.02614	29.95206
ASL	Marshall	−94.30778	32.52050
GLS	GALVESTON/SCHOLES	−94.86042	29.26533
ATA	Atlanta	−94.19530	33.10180
CNW	Waco	−97.07414	31.63781
GOP	GATESVILLE	−97.79697	31.42128
ILE	KILLEEN MUNI (AWOS)	−97.68650	31.08583
PIL	PORT ISABEL−CAMERON COUNTY APT	−97.33781	26.15970
BRO	BROWNSVILLE INTL	−97.42313	25.91461
PSN	PALESTINE	−95.70631	31.77969
TPL	TEMPLE/MILLER(AWOS)	−97.40778	31.15250
LVJ	Pearland Regional	−95.24170	29.51890
EDC	Austin	−97.56213	30.39255
PKV	PORT_LAVACA	−96.68100	28.65400
RKP	ROCKPORT/ARANSAS CO	−97.04639	28.08361
RFI	Henderson	−94.85172	32.14172
T20	Gonzales	−97.46140	29.52800
RBD	DALLAS/REDBIRD ARPT	−96.87000	32.68000
CRS	CORSICANA	−96.40000	32.03000
60R	Navasota	−96.11330	30.37190
GYF	Alaminos Canyon Block 857	−94.89800	26.12900
PEZ	Pleasanton	−98.51998	28.95419
JDD	MINEOLA/QUITMAN	−95.49648	32.74220

continued on next page

Table S1: Continued from previous page

ID	Station	Longitude	Latitude
11R	BRENHAM_MUNICIPAL_APT	−96.37417	30.21889
HYI	SAN MARCOS (AWOS)	−97.86300	29.89275
MWL	MINERAL WELLS MUNI	−98.06018	32.78161
COT	COTULLA MUNICIPAL	−99.21833	28.45667
UTS	HUNTSVILLE MUNICIPAL AIRPORT	−95.58717	30.74689
SGR	HOUSTON/HULL FIELD	−95.65653	29.62225
DFW	DALLAS/FT WORTH	−97.03800	32.89683
GGG	LONGVIEW/GREGG CO.	−94.71149	32.38401
DRT	DEL RIO INTL (AUT)	−100.92716	29.37421
T35	Cameron	−96.97110	30.87936
GDJ	GRANBURY	−97.81694	32.44442
SPS	WICHITA FALLS/SHEP	−98.49280	33.97860
SSF	SAN ANTONIO/STINSON	−98.47105	29.33698
LHB	HEARNE	−96.62000	30.87000
LXY	Mexia Limestone	−96.51450	31.64120
DTO	Denton	−97.20060	33.20500
TKI	MC KINNEY	−96.59000	33.18000
GVT	GREENVILLE/MAJORS	−96.06533	33.06784
IAH	Houston Intercontinental	−95.36070	29.98440
T74	Taylor	−97.44320	30.57260
ATT	Austin − City/Camp Mabry	−97.76042	30.32081
RAS	PORT ARANSAS/MUSTANG BEACH ARPT	−97.09000	27.81000
LRD	LAREDO INTL AIRPORT	−99.46153	27.54380
F05	VERNON	−99.28375	34.22567
BMQ	BURNET MUNICIPAL/KATE CRADDOCK	−98.23861	30.73893
GTU	GEORGETOWN (AWOS)	−97.67666	30.68083
FTW	FORT WORTH/MEACHAM	−97.36244	32.81978
HLR	FT HOOD AAF/KILLEEN	−97.71450	31.13870
TME	Houston Exec	−95.89789	29.80503
T70	Laughlin AFB	−100.48100	29.12600
AQO	LLANO_MUNI_ARPT	−98.66194	30.78361
GYI	SHERMAN/DENISON	−96.67367	33.71411
LNC	LANCASTER	−96.71905	32.57919
CWC	Kickapoo	−98.49040	33.85784
AXH	Houston SW	−95.47692	29.50614
AUS	Austin Bergstrom Intl	−97.66989	30.19453
AFW	Fort Worth − Alliance	−97.31788	32.97160
DWH	HOUSTON/D.W. HOOKS	−95.55624	30.06803
SAT	SAN ANTONIO INTL	−98.46978	29.53369
JWY	MIDLOTHIAN/WAXAC	−96.91250	32.45611
SEQ	Seguin Randolph AFB	−97.90830	29.56580
GRK	FORT HOOD/GRAY AAF	−97.83000	31.07000
TXW	Weslaco	−97.97310	26.17750
2R9	Kenedy	−97.86557	28.82499
DAL	DALLAS/LOVE FIELD	−96.85178	32.84711
SEP	STEPHENVILLE/CLARK	−98.17767	32.21533
81R	San Saba	−98.71700	31.23520
MNZ	Hamilton	−98.14864	31.66593
GKY	ARLINGTON (WAS F54)	−97.09428	32.66386
CLL	COLLEGE STATION	−96.36389	30.58806

continued on next page

Table S1: Continued from previous page

ID	Station	Longitude	Latitude
HOU	HOUSTON/WILL HOBBY	−95.28245	29.63747
0F2	Bowie	−97.77556	33.60167
LBX	ANGLETON/LAKE JACKS	−95.46208	29.10864
GLE	GAINESVILLE	−97.19694	33.65139
RPH	GRAHAM_MUNI_ARPT	−98.55500	33.11000
ABI	Abilene	−99.68209	32.41063
BWD	BROWNWOOD MUNICIPAL	−98.95650	31.79361
ORG	Orange	−93.80361	30.06918
DLF	LAUGHLIN AFB	−100.77797	29.35949
FTN	Carrizo Springs	−100.01880	28.20860
ERV	KERRVILLE MUNICIPAL	−99.08547	29.97667
FWS	DFW NEXRAD	−97.30332	32.57297
VAF	Boomvang	−94.62530	27.35360
CZT	Carrizo Springs	−99.82360	28.52220
XBP	Bridgeport	−97.82839	33.17533
APY	Zapata	−99.24891	26.96879
RND	RANDOLPH AFB	−98.28000	29.53000
TYR	TYLER/POUNDS FLD	−95.40239	32.35414
ACT	Waco	−97.22830	31.61797
BMT	Beaumont	−94.21510	30.07020
4F2	Carthage	−94.29880	32.17600
RYW	Lago Vista	−97.96589	30.49670
BKD	Breckenridge	−98.89100	32.71905
GUL	Gunnison (GoM)	−93.53830	27.30390
LZZ	Lampasas	−98.19589	31.10619
CFD	Brazos	−96.33140	30.71570
GYB	GIDDINGS−LEE_CNTY_ARPT	−96.98000	30.17000
LUD	DECATUR	−97.58050	33.25425
HBV	HEBBRONVILLE	−98.73694	27.34956
66R	Columbus	−96.51580	29.64110
CXO	CONROE/MONTGOMERY COUNTY AIRPORT	−95.41453	30.35236
BEA	Beeville	−97.79103	28.36187
TRL	TERRELL	−96.27000	32.71000
ETN	Eastland	−98.80980	32.41350
DZB	Horseshoe	−98.35876	30.52705
GPM	GRAND_PRAIRIE	−97.04692	32.69878
SJT	SAN ANGELO/MATHIS	−100.49500	31.35167
RWV	Caldwell	−96.70409	30.51547
SLR	SULPHUR_SPRINGS	−95.62000	33.16000
HHF	CANADIAN	−100.40400	35.89500
F46	Rockwall	−96.43549	32.93059
CVB	Castroville	−98.85090	29.34192
6P9	Ranger	−98.59475	32.43172
ADS	DALLAS/ADDISON ARPT	−96.83645	32.96856
GZN	Cisco	−99.02370	32.36580
JCT	JUNCTION (AMOS)	−99.76639	30.51083
COM	Coleman	−99.40361	31.84114
PRS	Presidio Lely	−104.36150	29.63420
T82	FREDERICKSBURG/GILLESPIE COUNTY	−98.90919	30.24325
F44	Athens	−95.82835	32.16385

continued on next page

Table S1: Continued from previous page

ID	Station	Longitude	Latitude
BBD	Brady	−99.32393	31.17929
SWW	SWEETWATER/AVENGER FIELD AIRPORT	−100.46656	32.46736
MCJ	Houston Dunn	−95.39500	29.71400
HHV	Hoover Diana	−94.68860	26.93920
BQX	Brazos 451	−95.72440	28.49360
F17	Center	−94.15640	31.83160
CDS	CHILDRESS MUNICIPAL	−100.28806	34.43389
JSO	JACKSONVILLE	−95.22000	31.87000
6R6	DRYDEN	−102.21291	30.04602
ECU	ROCKSPRINGS	−100.17385	29.94692
BGD	BORGER/HUTCHINSON	−101.39366	35.70089
E42	Spearman	−101.19450	36.22100
JXI	GILMER/FOX_STEPHENS_FIELD	−94.95000	32.70000
FST	FORT STOCKTON	−102.91667	30.91194
DYS	DYESS AFB/ABILENE	−99.85500	32.42100
GNC	Seminole	−102.65267	32.67533
LBB	LUBBOCK INTL ARPT	−101.82278	33.66364
PEQ	PECOS	−103.51000	31.38000
MAF	Midland Intl	−102.20745	31.94662
BPG	BIG_SPRING	−101.52164	32.21261
OZA	Ozona	−101.20297	30.73528
5C1	San Antonio	−98.69464	29.72393
INK	WINK/WINKLER CO.	−103.20000	31.78000
SOA	SONORA MUNI	−100.64856	30.58569
T89	Castroville	−98.85090	29.34190
E11	Andews	−102.52950	32.33110
SNK	SNYDER	−100.95047	32.69339
ODO	ODESSA−SCHLEMEYER FLD (WAS E02)	−102.38667	31.92056
E41	Big Lake Reagan	−101.47250	31.19890
BIF	Fort Bliss	−106.38004	31.84953
ELP	EL PASO INTL ARPT	−106.37583	31.81111
AMA	AMARILLO ARPT(AWOS)	−101.70592	35.21936
VHN	Van Horn	−104.78380	31.05780
MDD	MIDLAND	−102.10103	32.03653
BPC	Pampa	−101.03014	35.88928
LLN	Levelland	−102.37250	33.55250
PVW	PLAINVIEW	−101.71734	34.16815
HRX	Hereford	−102.32641	34.85776
DHT	DALHART MUNICIPAL	−102.54728	36.02259
LUV	Lamesa	−101.92020	32.75630
DUX	DUMAS	−102.01300	35.85800
E38	ALPINE	−103.68400	30.38400
PPA	PAMPA	−100.99625	35.61300
MRF	MARFA MUNI (AMOS)	−104.02000	30.37000
GDP	GUADALUPE PASS AMOS	−104.80978	31.83312
PYX	PERRYTON/OCHILTREE COUNTY APT	−100.75000	36.41400
TFP	Ingleside	−97.21150	27.91303

end of table

References

Gagge, A. P., J. A. J. Stolwijk, and Y. Nishi, 1972: An effective temperature scale based on a simple model of human physiological regulatory response. *ASHRAE Transactions*, **7 (Part I)**, 247–262.

Lu, Y.-C. and D. M. Romps, 2022: Extending the heat index. *Journal of Applied Meteorology and Climatology*, **61 (10)**, 1367–1383.

Rothfusz, L. P., 1990: The Heat Index "equation" (or, more than you ever wanted to know about Heat Index). Technical Attachment SR 90-23, NWS Southern Region Headquarters, Forth Worth, TX.

Steadman, R. G., 1979: The assessment of sultriness. Part I: A temperature-humidity index based on human physiology and clothing science. *Journal of Applied Meteorology*, **18 (7)**, 861–873.